Bistability Analysis of Thermal Effects in Nonlinear Microresonator Waveguide

Nurul Fathinah Azrisham, Mohammad Amirul Hairol Aman and Ahmad Fakhrurrazi Ahmad Noorden[*]

Centre for Advanced Optoelectronics Research (CAPTOR), Kulliyyah of Science, International Islamic University Malaysia, Pahang, Malaysia

Corresponding author: fakhrurrazi@iium.edu.my

ABSTRACT

An analytical simulation of a nonlinear all-pass microring resonator (MRR) was performed based on ambient temperature and ring radius variation. The optical transfer function (OTF) of the MRR was obtained using the coupling theory formulation. The OTF was used to simulate the output spectrum of the MRR system. In this research, the thermal and ring radius effects on the bistable spectrum of the system were analyzed because low thermal stability and big ring radius are major impediments to utilizing bistability properties for various applications. The optimization of the bistable spectrum was executed by determining the suitable configuration of MRR based on the variation of temperatures and ring radii to obtain the largest switching power. The simulation results demonstrate that the MRR system using the ring radius of 3 µm at the temperature of 300 K yields the highest switching power with the optimized system. The optimization analysis was further done by investigating the solution for the MRR system when using a large ring radius and at low temperatures, which is a problem in achieving better bistability performance.

Keywords: *All-pass ring resonator, optical bistability, thermal bistability, switching power*

INTRODUCTION

Optical microresonators have made numerous research progresses in various aspects of the optical science field, such as nonlinear optics, optomechanics, quantum optics, and information processing [1, 2]. It is also one of the primary constituents for a wide range of photonics applications such as lasers [3], amplifiers [4], sensors [5], optical channel dropping filters (OCDFs) [6], optical add/drop (de)multiplexers (OADMs) [7], switches [8], routers, logic gates [9], and artificial media [10]. The concept of a small modal volume with significant light confinement has made all the applications above achievable. Microresonators are constructed to accommodate a spectrum of optical modes with specified polarisation, frequency, and field patterns by modifying their shape, size, and material composition.

Currently, the most well-known traveling wave-integrated optical resonators are the microring (MR) [11 – 15] and whispering gallery (WG) [2, 1] microresonators. The MRR has a basic configuration comprised of a ring-shaped waveguide linked to one bus waveguide. In MRR, the evanescent coupling occurs on closely spaced optical waveguides, which enable the light to transfer across waveguides [1]. The MRR also covers various optical properties, such as optical bistability [17], chaotic [18], and bifurcation [19] in nonlinear optics applications.

The optical bistability of a system happens when it has two output states for the same input value throughout a specific range of input values. A Fabry-Perot inter-ferrometer with a saturable absorber is an example of an optical bistability system [20]. Furthermore, optical bistability is an essential physical feature that leads to all-optical logic gates operation [9]. Many approaches to obtaining optical nonlinearity have been performed, including carrier-plasma dispersion [15], the optical Kerr effect, saturable absorption [21], and the thermo-optic effect [2], which typically manifest only when a high optical power density is achieved [9]. Besides that, all-optical functionality, such as logic operations, modulation, switching, and memory, can be achieved via optical bistability.

In addition, the dependency of optical bistability on linear and nonlinear variables, such as the coupling coefficients [11], effective free carrier lifetime [22], free carriers absorption [23], and thermo-optic effect [2], was usually discussed in the research field of MRR. The resonance wavelength of a microresonator changes with the development of optical power in the resonator because silicon's refractive index can vary directly or indirectly due to incident light intensity. This creates a positive feedback process, allowing the resonator to function as a bistable switch with two states: (1) off-resonance or "empty" and (2) on-resonance or "loaded" [17]. Nevertheless, applying optical bistability properties reduces its performance in the waveguide's low thermal stability system and big ring radius.

In this research, a mathematical-based simulation system was constructed to analyze the effect of temperature and various ring radii on the optical bistability of the MRR waveguide. The simulation system was developed by using Octave. The thermal and ring radius effects on the bistable spectrum of the MRR system were analyzed by varying the wavelength of the MR waveguide from 0.5 to 2.5 µm. The MRR consists of nonlinear core materials such as silicon. The system was analyzed based on various ambient temperatures and different ring radii of the MRR ranging from 50 to 300 K and 2 to 7 µm, respectively. Then, the optimized configuration of the MRR was investigated to achieve better bistability performance.

EXPERIMENTAL

Derivation of OTF for All-Pass MRR

The fundamental relations between the incident field, E_{in}, and transmitted field, E_{out}, through the bus waveguide and the circulating field, E_1 and E_2, through the ring waveguide, are obtained by combining relations of the coupler with the feedback path. The derivation of OTF is calculated using the scattering matrix through the correlations between the field from the coupling region and the input fields, as in Equation 1 [10].

$$\begin{pmatrix} E_1 \\ E_{out} \end{pmatrix} = \begin{pmatrix} C & iS \\ iS & C \end{pmatrix} \begin{pmatrix} E_2 \\ E_{in} \end{pmatrix} \qquad \text{Equation 1}$$

The matrix in Equation 1 can be expressed in a set of two linear equations in Equations 2 and 3:

$$E_1 = CE_2 + iSE_{in} \qquad \text{Equation 2}$$

$$E_{out} = iSE_2 + CE_{in} \qquad \text{Equation 3}$$

Where E_2 can be represented in terms of E_1 through phase shift as in Equation 4:

$$E_2 = \xi E_1 \qquad \text{Equation 4}$$

Equations 2,3 and 4 are solved to obtain an expression for the incident field, E_{in}, as in Equation 5:

$$E_{in} = \frac{E_1(1 - \xi C)}{iS} \qquad \text{Equation 5}$$

where self-coupling, C, is denoted in Equation 6 [24],

$$C = \sqrt{1 - \kappa}\sqrt{1 - \gamma} \qquad \text{Equation 6}$$

and cross-coupling, S is given by Equation 7 [24],

$$S = \sqrt{\kappa}\sqrt{1 - \gamma} \qquad \text{Equation 7}$$

Given phase shift as explained by Equation 8 [24],

$$\xi = \exp\left(\frac{-\alpha L}{2}\right)\exp(ikn_{total}L) \qquad \text{Equation 8}$$

where the output from port E_1 into port E_2 is connected by the feedback path in which the optical cavity length, $L = 2\pi R$, and the coefficient, k, is associated with wavelength as shown in Equation 9:

$$k = \frac{2\pi}{\lambda} \qquad \text{Equation 9}$$

Hence, by solving Equations 2,3,4 and 5, the expression for the ratio of the incident field, E_{in}, to the transmitted field, E_{out}, is obtained as in Equation 10 [24]:

$$OTF = \frac{E_{out}}{E_{in}} = \frac{C - \xi(1-\gamma)}{1 - \xi C} \qquad \text{Equation 10}$$

To calculate the output power, P_{out} for the simulation of the output spectrum for the nonlinear microresonator, the transmitted field, E_{out} is squared as in Equation 11 [12]:

$$P_{out} = |E_{out}|^2 \qquad \text{Equation 11}$$

Total Refractive Index of MRR

The total refractive index   of the MRR is formulated by considering the changes in the refractive index inside the system, as depicted in Equation 12. The three contributing factors include refractive index induced by the Kerr effect, Δn_K, Δn_T induced by the thermal effect, and Δn_{fcd} induced by the free carrier dispersion, as expressed in Equation 13 [25].

$$n_{total} = n_o + \Delta n \qquad \text{Equation 12}$$

$$\Delta n = \Delta n_K + \Delta n_T + \Delta n_{fcd} \qquad \text{Equation 13}$$

The value of n_o is 2.4, the transverse mode (TE) effective index of the silicon MRR at a wavelength of 1565.25 nm [25]. In this research, the only refractive index changes used were Δn_T and Δ_{cd} because both are related to the two-photon absorption (TPA), which can produce free carriers to change the refractive index, and the energy released during the carrier recombination process, is transformed to thermal energy [25]. Δn_K was ignored in this work because it only induces minimal change to the refractive index compared to Δn_T and Δn_{eed} [25]. The Equation for Δn_T, which is the relationship between temperature and thermo-optic coefficient of silicon and Δn_{fcd}, is represented by Equations 14 and 15, respectively.

$$\Delta n_T = (1.86 \times 10^{-4})T \qquad \text{Equation 14}$$

$$\Delta n_{fcd} = -\frac{q^2 N}{2\omega^2 \varepsilon_o n_o}\left(\frac{1}{m_{ce}} + \frac{1}{m_{ch}}\right) \quad \text{Equation 15}$$

Optimization of Bistable Spectrum of MRR

The optimization of the bistable spectrum of the system is determined based on the value of the switching power and hysteresis width [11]. The switching power, ΔP_{switch}, is calculated by subtracting the initial point from the final point for each loop on the y-axis, i.e., the output power values. Meanwhile, the value of the hysteresis width, W_{hys}, is computed by subtracting the initial point from the final point for each loop on the x-axis, i.e., the input power values. The following equations denote the corresponding formula for the calculations. The highest switching power values will give the hysteresis loop's highest properties [11]. The calculation of hysteresis width is crucial to determine the acceptable loops to be considered in the calculation. If the width is too small, then it is insignificant.

$$\Delta P_{switch} = P_{out2} - P_{out1} \qquad \text{Equation 16}$$

$$W_{hys} = P_{in2} - P_{in1} \qquad \text{Equation 17}$$

RESULTS AND DISCUSSION

Analysis of the Bistable Spectrum of MRR

The bistable output spectrum was simulated by plotting the graph of output power against input power with (a) a ring radius of 2 μm while varying the value of temperature from 50 to 300 K with the increment of 50 K and (b) at an ambient temperature of 100 K while varying the value of ring radius from 2 to 7 μm with the increment of 1 μm (Figure 1). The input spectrum of the graphs in Figure 1 was validated by comparing it with the literature [25]. The shape distribution of the simulated input spectrum is acceptable and close to the existing paper, as shown in Figure 2. The input power and wavelength differences were due to the different materials used in this research work and the selected previous literature.
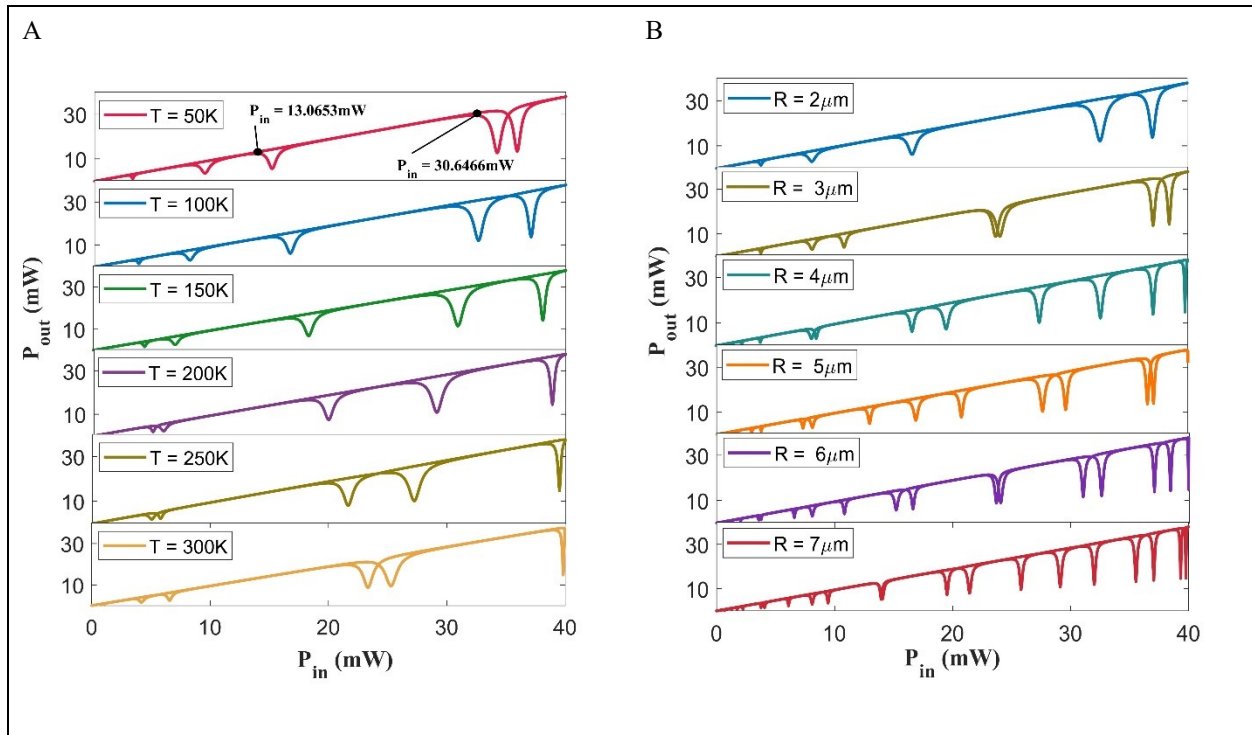
Figure 1: A) Bistable output spectrum varying in temperature with *R* = 2 μm and B) bistable output spectrum varying ring radius with *T* = 100 K.
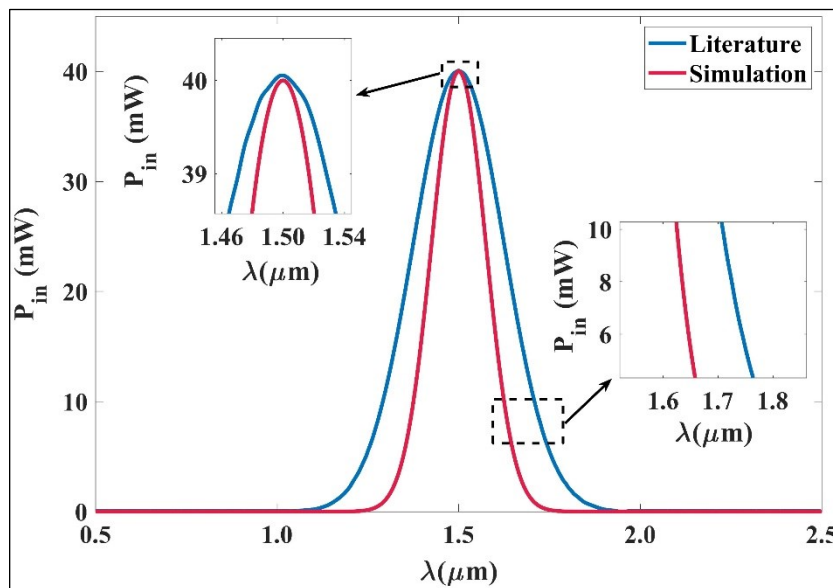

Figure 2: Validation of input spectrum between existing literature and simulated data.

Figure 1A shows the relationship between the system's output power and input power varying in ambient temperature. The figure shows that the number of hysteresis loops remained the same when the system's ambient temperature increased. However, the loops moved towards and from each other. Based on the significant butterfly hysteresis loop initially formed at the input power of 30.6466 mW when the ambient temperature was 50 K, the distance between the loop pair increased as the ambient temperature increased. However, when the ambient temperature was 50 K, the bistability loop formed at the input power of 13.0653 mW started to form a butterfly hysteresis loop with the neighboring loop as the temperature increased. Meanwhile, the bistability loops formed at the input power lower than 10 mW were negligible because the loops were too small to decipher. It is observed that the width and height of the loops are approximately the same at any temperature.

This condition happened due to the thermo-optic effect $(\frac{dn}{d})$, which represents the dependence of material refractive index on temperature [2]. According to the resonance condition $2\pi n(T)R(T) = m\lambda(T)$, temperature changes will affect the system's wavelength, which results in changes in the material refractive index [2]. Hence, it can be expressed that the MRR wavelength is a linear function of the refractive index, which varies with the environment's temperature. Therefore, it can be said that MRR with a more significant thermo-optic coefficient usually leads to a more significant frequency shift [2]. The temperature of the MRR system can be adjusted by an external thermal source or heat produced from optical absorption [2]. This method is widely used in applying thermal sensing and resonance frequency tuning, including tunable microlasers [26] and optical filters [27].

Figure 1B shows the relationship between the input power and output power of the system's varying ring radius. The figure shows that the number of bistable hysteresis loops increased as the radius of the ring resonator increased. Based on Figure 1b), the width of the loops decreased while the height was approximately the same as the radius increased. There is a significant distortion of the bistable loop generated when simulated using the radius of 3 and 6 μm at an input power of 23.8 mW. The formation of the butterfly hysteresis loop at the radius of 7 μm was challenging to distinguish compared to other graphs due to the large number of loops that have become crowded. The larger the number of hysteresis loops, the narrower the width and the higher the height of the loops.

According to the Equation of optical cavity length, $L = 2\pi r$, any changes in the ring radius's value will affect the optical cavity's length. This circumstance will change the magnitude of the phase shift, where it contributes to the changes in the formation of the bistable spectrum, such as the number of hysteresis loops, width, and height of the respected loops, through the Equation of output electric field and output power. Reducing the size of the ring radius exhibits wider hysteresis width due to the more robust optical phase modulation in the active region and stronger intensity-dependent nonlinear refractive index [28].

Optimization of Bistable Spectrum

The optimization of the bistable spectrum was analyzed by calculating the switching power and the hysteresis width of the bistable loops.

Table 1: Switching power data with the ring radii and ambient temperature variation.

| Radius (μm) | Switching power (mW) | | | | | |
| | Temperature (K) | | | | | |
	50	100	150	200	250	300
2	16.8037	20.6325	21.6651	22.4388	23.1933	23.3132
3	22.2164	20.4655	20.6307	19.9917	22.7122	23.3466
4	19.6373	21.0303	21.7844	21.9060	21.2537	20.4883
5	21.0186	20.3249	19.7576	22.2737	19.1315	20.2827
6	20.0762	21.1821	21.1499	20.4112	19.5364	20.8789
7	14.1063	20.0305	21.7029	19.8220	16.8690	19.9648

Table 1 shows that the switching power values were approximately the same for every ring radius, and there was no consistent pattern for each ring radius at any temperature. However, at the radii of 2 and 7 μm, the switching power decreased at every temperature except at the ambient temperature of 150 K, where it increased, and it is noted that the difference between the values was minimal. The highest switching power of 23.3466 mW was generated when simulated with a ring radius of 3 μm at an ambient temperature of 300 K, and the smallest switching power of 14.1063 mW was generated with a ring radius of 7 μm at an ambient temperature of 50 K.

The smallest switching power generated with a ring radius of 7 μm at an ambient temperature of 50 K can be increased by decreasing the cavity size. Thus, higher switching power of 22.2164 mW can be achieved using a smaller cavity size of 3 μm. Meanwhile, the lowest switching power of 16.8037 mW was produced at an ambient temperature of 50 K with a ring radius of 2 μm. The switching power can be increased by increasing the ambient temperature to 300 K and therefore having a higher switching power of 23.3132 mW. A higher value in switching power is essential for better optical bistability performance [12].

Table 2 shows the value of hysteresis width with varying ring radius and ambient temperature. It is observed that the hysteresis width values decreased as the radius increased at every temperature, with minimal difference among the values. The inconsistent pattern of hysteresis width values was also noted when the temperature was varied for every ring radius. A comparison was made between the value of the width of the minor temperature, 50 K, and the highest temperature, 300 K. The width values decreased for any ring radius except ring radii of 5 and 7 μm. The highest value of hysteresis width was 11.6406 mW, formed when simulating the system using the ring radius of 2 μm at the ambient temperature of 50 K. Meanwhile, the simulation of the system using a ring radius of 7 μm at the ambient temperature of 50 K produced the lowest hysteresis width of 2.3637 mW.

Furthermore, at the ambient temperature of 50 K, the smallest hysteresis width of 2.3637 mW was formed using the ring radius of 7 μm. A bigger width size can be achieved by decreasing the ring radius, for example, by using a smaller cavity size of 2 μm and thus having a bigger width size of 11.6406 mW. Aside from having better optical bistability performance as one of the importance in producing bigger hysteresis width, configurations that can generate significant and substantial hysteresis loop width are more fitting to be used for all-optical switching application than to be used as a conventional all-pass MRR [12].

Table 2: Data of hysteresis width with the variation of ring radii and ambient temperatures.

Radius (μm)	Hysteresis Width (mW)					
	Temperature (K)					
	50	100	150	200	250	300
2	11.6406	8.6280	11.2918	11.2011	11.0709	10.3304
3	6.0304	6.7574	7.8502	7.9192	5.9351	5.8339
4	5.3070	5.2487	5.1909	5.2265	5.1647	5.2027
5	3.6480	4.3902	4.4823	3.5113	4.4163	4.4203
6	3.4302	3.4286	3.3333	3.3713	3.8625	3.3021
7	2.3637	3.0649	2.5184	3.0122	3.4135	2.9913

CONCLUSION

In conclusion, the OTF for the all-pass MRR was derived by the scattering matrix through the relationship between the field from the coupling region and the input fields. The bistable output spectrum was analyzed by manipulating the ambient temperature and ring radius. It is observed that the number of bistable loops was the same in every ambient temperature, but the loops moved towards and from each other. The changes in the hysteresis loops across each temperature were due to the thermo-optic effect, representing the dependency of material refractive index on temperature. When the bistable output spectrum was simulated by varying the ring radius, it was discovered that the number of hysteresis loops increases and becomes crowded as the radius increases. The larger the number of hysteresis loops, the narrower the width and the higher the height of the loops. The optimization of the bistable output spectrum was determined by the calculation of switching power and hysteresis width of the bistable loops. It is found that the most optimum bistable output spectrum from this simulation is the hysteresis loop that was generated using a ring radius of 3 μm and at an ambient temperature of 300 K, where the configuration produced the highest number of switching power. Thus, this research proves that achieving greater bistability performance can be hindered by low thermal stability and a big ring radius. A low switching power at any temperature can be increased by decreasing the cavity size of the ring resonator. Low switching power when using any ring radius can be increased by increasing the system's ambient temperature. Meanwhile, narrow hysteresis width at any temperature can be wider by decreasing the radius of the MRR. A higher value in switching power and wider hysteresis width is crucial for better optical switching performance.

ACKNOWLEDGMENTS

AUTHOR'S CONTRIBUTION

Nurul Fathinah conceptualized the research idea, carried out the research, designed it, and wrote the article. Mohammad Amirul provided the theoretical framework and aided in the numerical simulations. Ahmad Fakhrurrazi conceived the original idea, supervised the research progress, anchored the review, revised, and approved the article submission.

CONFLICT OF INTEREST STATEMENT

The authors declare no conflict of interest.

REFERENCES

[1] Boriskina, S. V. (2010). Photonic Microresonator Research and Applications. *Photonic Molecules and Spectral Engineering*, vol. 156.

[2] Jiang, X. and Yang, L. (2020). Optothermal dynamics in whispering-gallery microresonators, *Light: Science and Applications*, vol. 9, no. 1. doi: 10.1038/s41377-019-0239-6.

[3] Jin, L., Yang, Z., and Zhang, Q. (2019). Properties of Gaussian Beam Propagating in Ring Resonator Sensor. *International Journal of Optics*, vol. doi: 10.1155/2019/3573976.

[4] Kim, J. H. et al. (2004). All-optical logic gates using semiconductor optical-amplifier-based devices and their applications. *Journal of the Korean Physical Society*, vol. 45, no. 5 I.

[5] Ahmed, R., Rifat, A. A., Yetisen, A. K., M. Salem, M. S., Yun, S. H. and Butt, H. (2016). Optical microring resonator-based corrosion sensing. *RSC Advances*, vol. 6, no. 61. doi: 10.1039/c6ra11538a.

[6] Chen, G. and Jiang, C. (2020). Reverse design of microring resonator channel dropping filters. *Results in Physics*, vol. 19. doi: 10.1016/j.rinp.2020.103380.

[7] Wu, D., Wu, Y., Wang, Y., An, J., & Hu, X. (2016). Reconfigurable optical add-drop multiplexer based on thermally tunable micro-ring resonators. *Optics Communications*, *367*, 44–49. https://doi.org/10.1016/j.optcom.2016.01.018.

[8]   Tian, Y. et al. (2016). Reconfigurable electro-optic logic circuits using microring resonator-based Optical Switch Array. *IEEE Photonics Journal*, *8*(2), 1–8. https://doi.org/10.1109/jphot.2016.2524009.

[9]   Haret, L.-D., Tanabe, T., Kuramochi, E., & Notomi, M. (2009). Extremely low-power optical bistability in silicon demonstrated using 1D photonic crystal nanocavity. *Optics Express*, *17*(23), 21108. https://doi.org/10.1364/oe.17.021108.

[10]   Heebner, J., Grover, R., and Ibrahim, T. (2008). Optical Microresonators: Theory, fabrication, and applications. *Springer Series in Optical Sciences*, vol. 138.

[11]   Ahmad Noorden, A. F., Daud, S., Haider Rizvi, S. Z., Ali, J., & P. Yupapin, P. (2016). Optical bistability is controlled using an add-drop Mobius microring resonator system. *Jurnal Teknologi*, *78*(3). https://doi.org/10.11113/jt.v78.7504.

[12]   Ahmad Noorden, A. F., Bahadoran, M., Chaudhary, K., Aziz, M. S., Jalil, M. A., Ali, J., & Yupapin, P. (2015). Optical bistability in all-pass mobius configuration microring resonator. *Jurnal Teknologi*, *76*(13). https://doi.org/10.11113/jt.v76.5835.

[13]   Dunmeekaew, U., Tasakorn, M., Pornsuwancharoen, N., & Yupapin, P. P. (2009). New wavelength division multiplexing bands are generated by using a Gaussian pulse in a microring resonator system. *Physics Procedia*, *2*(1), 33–38. https://doi.org/10.1016/j.phpro.2009.06.006.

[14]   Zhou, J., Du, Q., Xu, P., Zhao, Y., Lin, R., Wu, Y., Zhang, P., Zhang, W., & Shen, X. (2018). Large nonlinearity and low loss Ge-SB-se glass photonic devices in near-infrared. *IEEE Journal of Selected Topics in Quantum Electronics*, *24*(4), 1–6. https://doi.org/10.1109/jstqe.2018.2827671.

[15]   Perron, D., Wu, M., Horvath, C., Bachman, D., & Van, V. (2011). All-plasmonic switching based on thermal nonlinearity in a polymer plasmonic microring resonator. *Optics Letters*, *36*(14), 2731. https://doi.org/10.1364/ol.36.002731.

[16]   Ramiro-Manzano, F., Prtljaga, N., Pavesi, L., Pucker, G., & Ghulinyan, M. (2013). Thermo-optical bistability with si nanocrystals in a whispering gallery mode resonator. *Optics Letters*, *38*(18), 3562. https://doi.org/10.1364/ol.38.003562.

[17]   Shankar, R., Bulu, I., Leijssen, R., & Lončar, M. (2011). Study of thermally induced optical bistability and the role of surface treatments in si-based mid-infrared photonic crystal cavities. *Optics Express*, *19*(24), 24828. https://doi.org/10.1364/oe.19.024828.

[18]   Tian, W., Zhang, L., Ding, J., Shao, S., Fu, X., & Yang, L. (2018). Ultrafast physical random bit generation from a chaotic oscillator with a silicon modulator. *Optics Letters*, *43*(19), 4839. https://doi.org/10.1364/ol.43.004839.

[19]   Coarer, F. D.-L., Sciamanna, M., Katumba, A., Freiberger, M., Dambre, J., Bienstman, P., & Rontani, D. (2018). All-optical reservoir computing on a photonic chip using silicon-based ring resonators. *IEEE Journal of Selected Topics in Quantum Electronics*, *24*(6), 1–8. https://doi.org/10.1109/jstqe.2018.2836985.

[20]   (1985). *Optical Bistability: Controlling Light with Light*. doi: 10.1016/b978-0-12-281940-7.x5001-x.

[21] Sodagar, M., Miri, M., Eftekhar, A. A., & Adibi, A. (2015). Optical bistability in a one-dimensional photonic crystal resonator using a reverse-biased PN-junction. *Optics Express*, *23*(3), 2676. https://doi.org/10.1364/oe.23.002676.

[22] Chiangga, S., Pitakwongsaporn, S., Frank, T. D., & Yupapin, P. P. (2013). Optical bistability investigation in a nonlinear silicon microring circuit. *Journal of Lightwave Technology*, *31*(7), 1101–1105. https://doi.org/10.1109/jlt.2013.2243819.

[23] Chen, S., Zhang, L., Fei, Y., & Cao, T. (2012). Bistability and self-pulsation phenomena in silicon microring resonators based on nonlinear optical effects. *Optics Express*, *20*(7), 7454. https://doi.org/10.1364/oe.20.007454

[24] Noorden, A. F., Mohamad, A., Salleh, M. H., Daud, S., Mohamad, S. N., & Ali, J. (2020). Free spectral range analysis of double series microresonator system for all-optical corrosion sensors. *Optical Engineering*, *59*(01), 1. https://doi.org/10.1117/1.oe.59.1.017106.

[25] Wang, Z., Liu, H., Sun, Q., Huang, N., Li, S., & Han, J. (2016). The influence of thermal and free carrier dispersion effects on all-optical wavelength conversion in a silicon racetrack-shaped microring resonator. *Laser Physics*, *26*(7), 075403. https://doi.org/10.1088/1054-660x/26/7/075403.

[26] Linslal, C. L., Kailasnath, M., Mathew, S., Nideep, T. K., Radhakrishnan, P., Nampoori, V. P., & Vallabhan, C. P. (2016). Tuning whispering gallery lasing modes from polymer fibers under tensile strain. *Optics Letters*, *41*(3), 551. https://doi.org/10.1364/ol.41.000551.

[27] Monifi, F., Friedlein, J., Ozdemir, S. K., & Lan Yang. (2012). A robust and tunable add–drop filter using a whispering gallery mode Microtoroid Resonator. *Journal of Lightwave Technology*, *30*(21), 3306–3315. https://doi.org/10.1109/jlt.2012.2214026.

[28] Qasaimeh, O. (2016). Bistability characteristics of different types of optical modes amplified by quantum dot vertical-cavity semiconductor optical amplifiers. *Optics Communications*, *364*, 115–122. https://doi.org/10.1016/j.optcom.2015.11.042.